Static properties of quantum spin S=1 chains: TMNB, TMNC and $CsNiF_3$

1992 J. Phys.: Condens. Matter 4 2915

(http://iopscience.iop.org/0953-8984/4/11/018)

J. Phys.: Condens. Matter 4 (1992) 2915–2926. Printed in the UK

Static properties of quantum spin $S = 1$ chains: TMNB, TMNC and $CsNiF_3$

L S Campana†, A Caramico D'Auria†, F Esposito†, U Esposito†, R W Gerling‡ and G Kamieniarz‡§

† Dipartimento di Scienze Fisiche, Universitá di Napoli, Piazzale Tecchio, 80125 Napoli, Italy

‡ Institut für Theoretische Physik I, Universität Erlangen-Nürnberg, Staudtstrasse 7, D-8520 Erlangen, Federal Republic of Germany

Received 6 February 1991

Abstract. The zero-field parallel and perpendicular susceptibility and the zero-field specific heat of the quantum easy-plane $S = 1$ Heisenberg spin chains are calculated numerically and applied to TMNB, TMNC and $CsNiF_3$. New values of the model parameters are estimated from fitting procedures. As to $CsNiF_3$, the in-plane specific heat, the field-dependent magnetization and the spin-wave dispersion are also evaluated for a given choice of the microscopic parameters ($J/k_B = 20.5$ K, $A/J = 0.425$) and compared with measured quantities. An overall agreement with experiment is revealed.

1. Introduction

Since the interpretation of solitons as quasi-particles [1] and the recognition of their role in the understanding of the thermodynamic properties of magnetic chains as well as the foregoing observation [2] of the central peak in the neutron scattering experiment on $CsNiF_3$, the quasi-one-dimensional magnetic systems have attracted a great deal of interest [3]. It has been shown under certain approximations [4] that the equation of motion of the spin chain described by the easy-plane Heisenberg model with the in-plane field can be mapped onto a classical sine-Gordon (sG) equation yielding linear and non-linear excitations.

A considerable amount of experiments [3] on quasi-one-dimensional magnetic systems with the easy-plane anisotropy has been performed and interpreted qualitatively by recourse to the sG model. However, some quantitative disagreement found for the specific heat and neutron scattering data [5–7], unknown effects of different approximations underlying the sG model, as well as controversies about the importance of the out-of-plane fluctuations versus the sG model quantization, have led to numerical simulations. In the quantum version they are based on the Suzuki–Trotter formalism [8] leading to the quantum Monte Carlo (QMC) [9–11] or to the quantum transfer matrix (QTM) techniques [10, 12]. The finite-size chain calculations have also been widely applied [11, 13–16]. On the classical level, the simulations have been performed

§ On leave of absence from the Institute of Physics, A. Mickiewicz University, 60-769 Poznań, Poland. Present address: Faculty of Applied Physics, TU Delft, Lorentzweg 1, The Netherlands.

0953-8984/92/112915+12$04.50

in the framework of the corresponding transfer matrix [17], Monte Carlo, or equation-of-motion technique [18].

Our results reported here are obtained within the finite-size chain method and refer to the following soliton-bearing systems: $(CH_3)_4NNiBr_3$ (TMNB), $(CH_3)_4NNiCl_3$ (TMNC) and $CsNiF_3$ which can be described by the Hamiltonian

$$\mathcal{H} = -J\sum_{i=1}^{N} \boldsymbol{S}_i \cdot \boldsymbol{S}_{i+1} + A\sum_{i=1}^{N}(S_i^z)^2 - g\mu_B B\sum_{i=1}^{N} S_i^\alpha \tag{1}$$

where J denotes the ferromagnetic coupling constant, A, the anisotropy parameter and B, the external magnetic field which can be applied in the chain direction ($\alpha = z$) or in the easy plane ($\alpha = x$).

In the previous paper [19] (denoted hereafter as I) we were concerned with the static properties of $CsNiF_3$ which is considered a good quasi-one-dimensional compound with $T_c = 2.7$ K and very weak interchain interactions. Assuming the commonly used parameters [20],

$$J/k_B = 23.6 \text{ K} \qquad A/k_B = 9.0 \text{ K} \qquad g = 2.4 \tag{2}$$

we considered in I longer (N up to 7 sites) spin chains than before [21] and we found an error in the $S = 1$ part of [21]. It turned out, however, that the excess specific heat maxima were not much improved (figures 1 and 2 in I). Somewhat better estimates of the excess specific heat $\Delta C(T,B) = C(T,B) - C(T,0)$ were also reported in I, but the anisotropy parameter was modified ($A/k_B = 6$ K) after [22]. To compare our predictions with the magnetization measurements, we adopted in I the value $g = 2.08$ reported in [23].

The aim of the present paper is a more coherent description of the compounds in question. First we fix theoretically the microscopic parameters in (1) from some fitting procedures and then we calculate a variety of static characteristics.

2. Fitting procedure

The coefficient $g\mu_B B/J$ of the third term in (1) amounts to 0.07 for $B = 1$ T and remains small in the experimental region of the applied fields so that we fit the parameters of the model Hamiltonian (1), searching for an overall agreement between our numerical estimates and the corresponding *zero-field* experimental data. To simplify the fit, the g-factors are kept constant and assume the values fixed in [24] from the resonance experiments. As to $CsNiF_3$, the g-factors are anisotropic and have the following values

$$g_{\|} = 2.23 \qquad g_{\perp} = 2.28 \tag{3}$$

where $\|$ and $\perp$ stand for the field directions with respect to the chain axis. The values in (3) fulfil $2.08 < g_{\|}, g_{\perp} < 2.4$, giving a good compromise between $g = 2.08$ [23] and $g = 2.4$ [20].

Our theoretical estimates have been found for finite chains with size up to $N_{max} = 8$ and up to $N_{max} = 7$ for the field applied in the z and x directions, respectively. After having diagonalized the matrix representation of (1), the corresponding

thermodynamic quantities have been evaluated in the standard way [15, 19, 21] for $2 \leqslant N \leqslant N_{max}$ and the linear extrapolations in $1/N$ have been performed. The error bars and the uncertainties have been estimated taking into account the variations of the extrapolated values with respect to the number of points as well as new parabolic extrapolations.

Extending the length of chains with respect to those in [19, 24], we have calculated the zero-field specific heat C, the parallel susceptibility $\chi_{\parallel}$ and the perpendicular susceptibility $\chi_{\perp}$, and we have compared them with the available zero-field experimental data [24, 25]. The model parameters chosen here yield the best overall fit. Due to the procedure adopted, our parameters should be close to those found in [24]. We emphasize, however, that $\chi_{\perp}$ plays an active role and was previously neglected [24] because of the lower symmetry of (1) for the in-plane field.

3. Results and discussion

In figures 1 and 2 $\chi_{\parallel}$ and $\chi_{\perp}$ are presented for TMNB. The experimental data [24] are shown by full squares and the theoretical estimates by full curves. Note that for all the compounds considered here, the g factors are unchanged and assume values assigned in [24], whereas the parameters J and A/J are subject to modifications according to the fitting procedure. The parameters yielding the best overall fit for TMMB are: $J/k_B = 10.0 \pm 0.5$ K, $A/J = 0.35 \pm 0.02$.

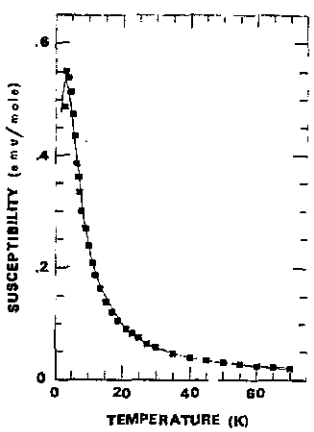

Figure 1. Fit of the susceptibility parallel to the chains $\chi_{\parallel}$ for TMNB. The full squares represent the experimental data and the curve represents the theoretical estimates.

Our results for TMNC are displayed in figures 3 and 4 for C and $\chi_{\parallel}$, respectively, and lead to the following interaction parameters: $J/k_B = 3.3 \pm 0.2$ K, $A/J = 1.1 \pm 0.1$. The curves for $\chi_{\perp}$ are not presented explicitly, as the agreement with experiment is even better than that shown in figure 2. Some systematic deviations occur only in the low-temperature region in the close vicinity of the 3D long-range-order critical point. For TMNC the experimental results have been fitted not only for $\chi_{\parallel}$ and $\chi_{\perp}$, but also for C. Again, $g_{\parallel}$ and $g_{\perp}$ are not the adjustable parameters so that the fit is carried out varying J and A/J.

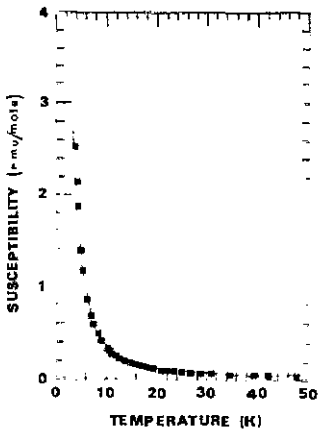

Figure 2. Fit of the susceptibility perpendicular to the chains $\chi_\perp$ for TMNB. The experimental and theoretical data are represented by the full squares and the curve, respectively.

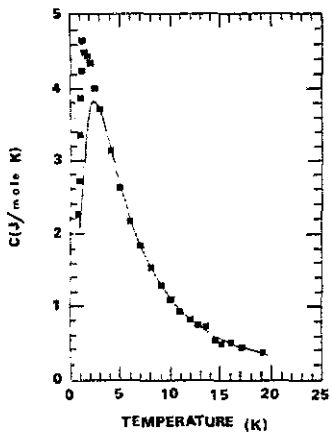

Figure 3. Fit of the theoretical curve to the zero-field experimental specific heat (full squares) for TMNC.

In view of an interest in $CsNiF_3$ and some discrepancies which have prevailed between theory and experiment ([19] and references therein), we find it important to determine new parameters of (1) for $CsNiF_3$ within our procedure and then to calculate the corresponding field-dependent characteristics. Unfortunately, reliable zero-field specific heat data are not available for $CsNiF_3$ so that we are confined to the zero-field susceptibility data [24] only. The latter, performed on the single crystal, are reported together with our theoretical predictions in figures 5 and 6. The g values are given in (3) and the best fit is reached for

$$J/k_B = 20.5 \pm 1.0 \text{ K} \qquad A/J = 0.425 \pm 0.15. \tag{4}$$

Due to systematic underestimations of $\chi_\perp$ observed in figure 6, we were prompted to search for a somewhat modified set of parameters, relaxing our condition that g should be kept constant. The result for $\chi_\parallel$ is presented in figure 7 by the full curve.

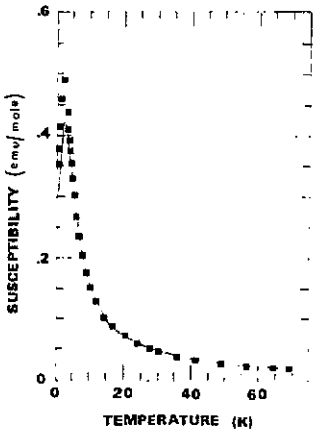

Figure 4. Fit of $\chi_{\|}$ with theory for TMNC.

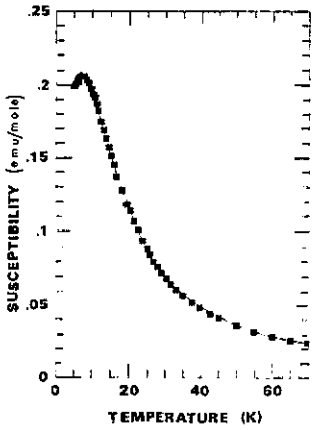

Figure 5. Fit of $\chi_{\|}$ with theory for $CsNiF_3$ and parameters (3)-(4).

This fit is found for the alternative set of the parameters

$$J/k_B = 26.5 \text{ K} \qquad g_{\|} = 2.07 \tag{5}$$

having assumed *ad hoc* that $A/J = 0.3$. The fit is nearly as good as that in figure 5. It turns out, however, that the values of the parameters J and g given by (5) do not improve the low-temperature behaviour of $\chi_{\perp}$. Though the parameter $g_{\|} = 2.07$ is close to the corresponding value inferred from the saturation magnetization measurements [23], there is also experimental evidence supporting the value $g = 2.4$ [20] found from the low-temperature powder susceptibility measurements. The result in (5) demonstrates the ambiguity in the fitting procedure. It is interesting that some very recent neutron scattering experiments [26] have confirmed the previous findings [27] for the parameters

$$J/k_B = 23.0 \pm 0.1 \text{ K} \qquad A/k_B = 8.9 \pm 0.2 \text{ K} \tag{6}$$

which almost coincide with those in (2).

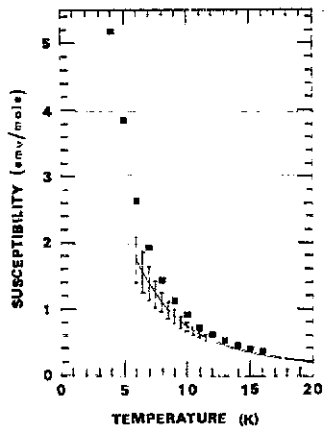

Figure 6. Fit of $\chi_{\perp}$ with theory for $CsNiF_3$. Our estimates are supplemented by error bars.

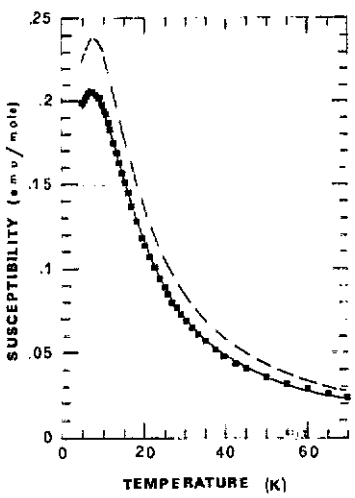

Figure 7. Fit of $\chi_{\parallel}$ with theory for $CsNiF_3$. The full curve represent predictions for the parameters given by (5) and the broken curve, for the parameters given by (6).

Before discussing the different predictions (4)–(6) for $CsNiF_3$ microscopic parameters, we present our results for the static field-dependent properties which compare rather well with the corresponding measurements. We consider the microscopic parameters (3)–(4) in our calculations of the remaining field-dependent characteristics of $CsNiF_3$.

We have found in the excess specific heat data $\Delta C(T, B)$ well-defined maxima for any given temperature. The heights of the peaks $\Delta C_m(T)$ and the peak positions $B_m(T)$ are reported in figures 8 and 9, respectively. The experimental data [6] are denoted by full and open circles, the QMC predictions by open triangles, and our estimates by crosses. Our present results are superior to those found previously [10, 19, 21].

We note that the g value has no effect on $\Delta C_m(T)$, and according to an analysis performed in I, the uncertainties of our extrapolations are of the order of 10% at

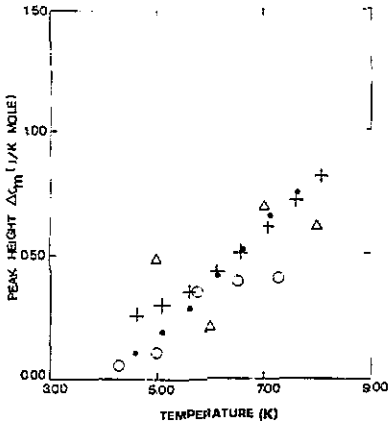

Figure 8. The excess specific heat maxima $\Delta C_m(T)$ as a function of temperature. Experimental data are reported by the circles (solid for the new disk-shaped sample and open for the older sample). The open triangles represent the QMC predictions. Our estimates are shown by crosses.

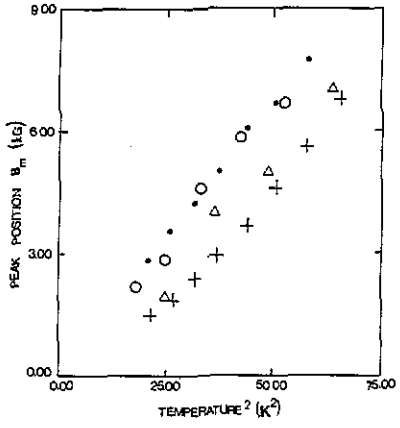

Figure 9. Peak positions $B_m(T)$ of the excess specific heat as a function of the square of temperature. The solid and open circles represent the experimental data for the new disk-shaped sample and the older sample, respectively. The open triangles represent the QMC predictions, whereas our estimates are shown by crosses.

lower temperatures and they are even smaller at higher temperatures. With respect to the peak position, the heat capacity measurements [6] are confined to a region of the (B,T) plane that is relatively close to $T_N(0)$. As the interchain interactions are antiferromagnetic, they tend to decrease the effect of an applied magnetic field. The magnetic phase diagram determined in [29] indicates that these interactions, expressed in terms of a field, amount to 2.1 kG. This agrees very nicely with the shift between the calculated and experimental results in figure 9. Some unexpected decrease of the shift appears for $T \leqslant 5$ K, where the limit of our extrapolation procedure is reached, and they are less reliable. Within this mean-field-like approach, the interchain interactions will hardly affect the comparison between theory and experiment presented in figure 8,

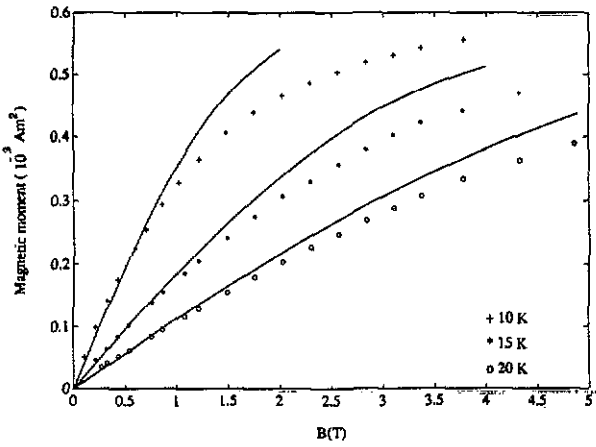

Figure 10. The in-plane magnetic moment versus the field at a given temperature. The symbols represent the experimental observations. The theoretical results are plotted by the curves.

since in that case the magnitude of the field is irrelevant.

The comparison with the magnetization measurements is shown in figures 10 and 11. The experimental magnetic moment isotherms [19,28] are reported by the symbols and our estimates by the full curves. Our g values (3) are higher than $g = 2.08$ quoted in [23] so that we are left with the part of the (B,T) plane outside the saturation region. The measurements were performed on two different samples [19,28]. The in-plane field was applied on the sample of $m = 14.5$ mg whereas the field parallel to the chain axis was applied on the sample of $m = 108.3$ mg. We find the overall agreement with experiment both for the in-plane and for the out-of-plane magnetic moment. It is likely that our magnetization profiles in figure 10 are not affected by the interchain interactions even in the low-field limit, as the temperatures considered are high enough ($T \geqslant 10$ K).

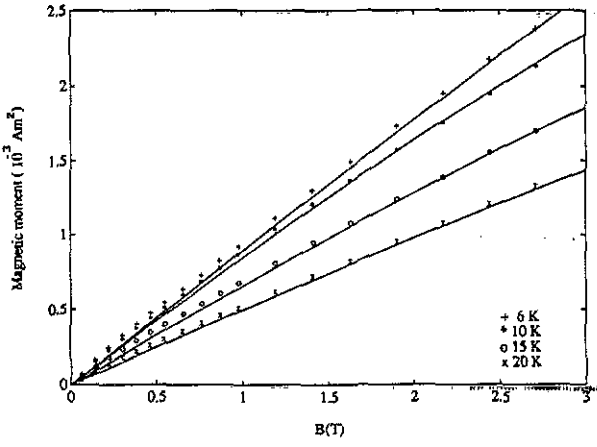

Figure 11. Magnetic moment versus the magnetic field applied along the chain axis. The symbols represent the experimental data, whereas the theoretical results are plotted by the curves.

In the remaining part of this section some implications of the different parameter choices (2)–(6) are discussed. As far as susceptibility is concerned, we have mentioned that our results (4) and (5) yield similar fit, although the latter slightly underestimate the experimental findings at higher temperatures. The susceptibility fit is very sensitive to the g value in the entire temperature region ($\chi \sim g^2$), and is also sensitive to other parameters at lower temperatures. At higher temperatures, however, the uncertainties of our extrapolations are lower than the experimental errors and even small systematic deviations from the experimental data present a strong argument against the corresponding parameters. On that basis Dupas and Renard [24] found the values close to (4) superior to (2) and (6). We have confirmed their conclusions. In figure 7 the susceptibility $\chi_{\parallel}$ for the parameters (6) and $g = 2.4$ is depicted by the broken curve. It strongly disagrees with the experimental results represented by the squares. Although the agreement can be improved if g is diminished, some systematic deviations prevail at higher temperatures.

The set (J, A, g), found from the zero-field $\chi_{\parallel}$ and $\chi_{\perp}$ data available for $CsNiF_3$, is somewhat ambiguous. The solution (4) was found for fixed values (3) of g, whereas solution (5) was for the fixed value $A/J = 0.3$. The zero-field specific heat C does not depend on g and the corresponding experimental data could help resolve the ambiguity. For that reason in figure 12 the zero-field specific heat curves are plotted for parameters (4)–(6). The results show that measurements of C with the accuracy of the order of 1–3% are required. From figure 12 we see that set (5) gives very flat temperature dependence above the maximum at 10 K. Our preferable set (4) leads to the maximum of C at 9 K and the temperature behaviour which could be distinguished from that for set (6), especially at low temperatures. In table 1 we report explicitly the variation of the C maxima with the number of points taken into account in the extrapolations. The maxima are very stable and we estimate the uncertaities for those temperatures at 0.1–0.3%, well below the required accuracy of the experimental data. Similar zero-field specific heat measurements performed on the spin-$\frac{1}{2}$ compound CHAB [12, 14, 16] turned out to be very helpful in matching the microscopic parameters.

Table 1. Distribution of the extrapolated maxima of the zero-field specific heat versus the number of points.

n	$A = 0.425$ $T_{max} = 9.0$	$A = 0.387$ $T_{max} = 10.0$	$A = 0.300$ $T_{max} = 10.0$
2	2.98832	2.90610	2.68829
3	2.98823	2.90595	2.68826
4	2.98887	2.90637	2.68795
5	2.98259	2.89961	2.67432
6	2.98360	2.89892	2.68837

The most direct method of fixing the microscopic parameters J and A is the neutron scattering experiment. The values quoted in (2) and (6) were determined, measuring the spin–wave dipersion relation. We emphasize, however, that our one-dimensional system (1) does not display the long-range order and the spin–wave theory is not as well established as for the conventional ferromagnets. In particular, the standard Holstein–Primakoff transformation is not applicable here and violates the Goldstone theorem which holds for the easy-plane anisotropic model (1). Instead, the Villain transformation [30] for the classical counterpart of (1) was applied and a

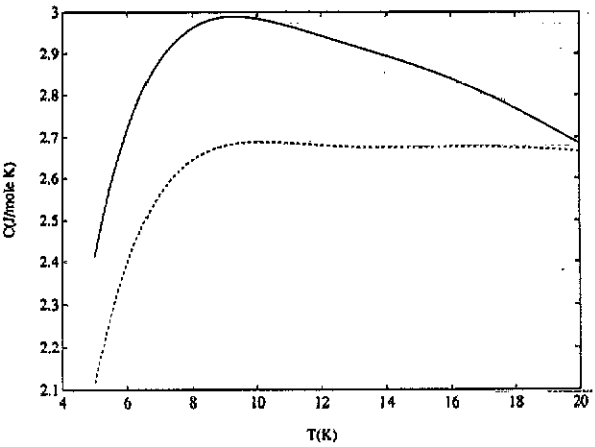

Figure 12. The theoretical zero-field specific heat. The predictions for the set (4) are plotted by the full curve, and those for the set (5) and (6) by the broken and dotted curves, respectively.

matching matrix element (MME) method [31] was devised for the quantum Hamiltonian (1). The former [20] led to the parameters (2) and the latter [26,27] led to the parameters (6). The MME approach pertains to 3D magnets and may be regarded as an expansion in $1/zS$, where z is the coordination number and S is the spin value. In the particular case of (1), the expansion parameter $d = A/(4SJ + g\mu_B B) \simeq 0.2$ remains small for the linear system and the Goldstone theorem is fulfilled up to the second order in d. Thus, the microscopic parameters J and A are fixed in the neutron scattering experiment, fitting the observed energy spectra to the theoretical dispersion relation E_q which is obtained perturbatively and gives the correct limit $E_q \to 0$ as $q \to 0$ up to the second order in d. Moreover, the experiments are performed at finite temperatures ($T = 4.2$ K) whereas the zero-temperature relation is referred to. At $k_B T/J = 0.2$ the reliable numerical simulations [18] show for the XY model about 5–8% reduction of the dispersion relation with respect to the zero-temperature predictions (figure 9 in [18]). Similar estimates (8–10%) have been found [32] for the dispersion of the classical counterpart of (1). In conclusion, parameters (2) and (6) are subject to some uncertainties, too.

Finally, we plot the corresponding spin-wave dispersions for the parameters (4) and (5) in figure 13, and the field dependence of the energy gap at the center of the Brillouin zone $q = 0$ in figure 14. The symbols denote the experimental [27] observations whereas the full and the broken curves denote the results for the parameters (4) and (5), respectively. For the dispersion we see deviations of the order of 10% in both cases. In the latter case they are more pronounced: for small q we find underestimations and for large q we find overestimations. As far as the $q = 0$ energy gap is concerned, our parameters (4) yield (figure 14) quantitative agreement with the FMR experiment (the data after figure 5(a) in [27]).

4. Conclusions

We have successfully applied the finite-size numerical approach to the title compounds TMNB, TMNC and $CsNiF_3$. We have applied the fit to the zero-field susceptibility and

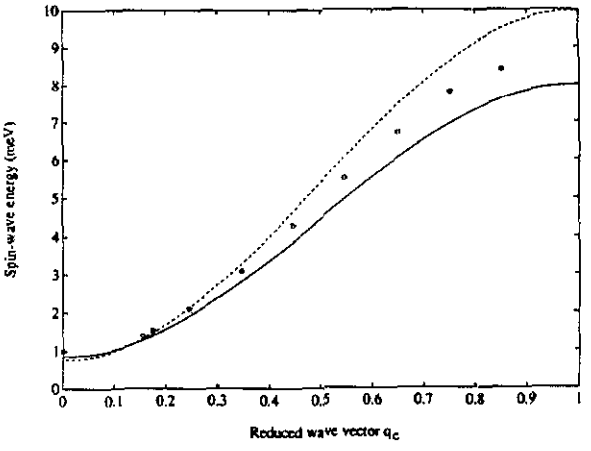

Figure 13. Spin-wave spectra. The experimental dispersion of the magnons in $CsNiF_3$ at 4.2 K at $B = 4.1$ T is shown by the symbols. The theoretical zero-temperature estimates for the parameters (4) and (5) are given by the full and broken curves, respectively.

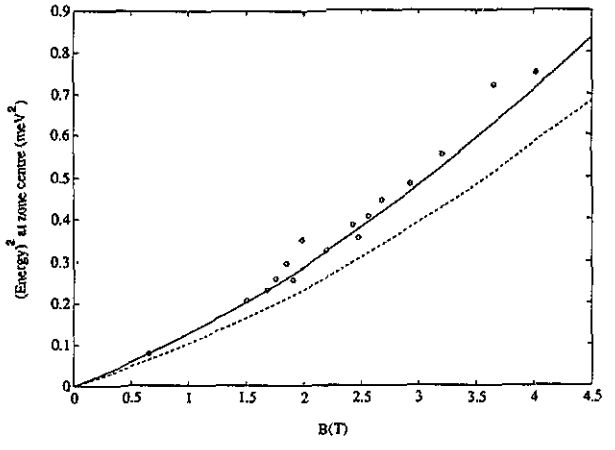

Figure 14. The energy gap $E^2_{q=0}$ versus magnetic field. The notation as in figure 13.

the zero-field specific heat (if available) data to fix the microscopic parameters. We have considered longer chains and the perpendicular susceptibility $\chi_\perp$, too.

Particular attention has been focused on $CsNiF_3$ to explain coherently its static properties by recourse to the model (1) with parameters (3) and (4). An overall quantitative agreement with experiment has been accomplished, although for the spin-wave dispersion systematic 10% deviations have been concluded.

Implications of the different parameter values have been extensively discussed and a new specific heat experiment has been suggested to overcome some ambiguities.

Acknowledgments

G K would like to thank the Alexander von Humboldt Foundation for a fellowship

supporting this research as well as Professors B Dorner, K Kopinga and H Leschke for valuable discussions.

References

[1] Krumhansl J A and Schrieffer J R 1975 *Phys. Rev.* B **11** 3535
[2] Kjems J K and Steiner M 1978 *Phys. Rev. Lett.* **41** 1137
[3] *Magnetic Excitations and Fluctuations* 1984 ed S W Lovesey, U Balucani, F Borsa and V Tognetti (Berlin: Springer)
Magnetic Excitations and Fluctuations II 1987 ed U Balucani, S W Lovesey, M G Rasetti and V Tognetti (Berlin: Springer)
[4] Mikeska H J 1978 *J. Phys. C: Solid State Phys.* **11** L29
Magyari E and Thomas H 1982 *J. Phys. C: Solid State Phys.* **15** L333
[5] Steiner M, Kakurai K and Kjems J K 1983 *Z. Phys.* B **53** 117
[6] Ramirez A P and Wolf W P 1985 *Phys. Rev.* B **32** 1639
[7] Tinus A M C, de Jonge W J M and Kopinga K 1985 *Phys. Rev.* B **32** 3154
[8] Suzuki M 1976 *Prog. Theor. Phys.* **56** 1454
[9] Cullen J J and Landau D P 1983 *Phys. Rev.* B **27** 297
[10] Wysin G and Bishop A R 1986 *Phys. Rev.* B **34** 3377
Satija I, Wysin G and Bishop A R 1985 *Phys. Rev.* B **31** 3205
[11] Kamieniarz G, Mallezie F and Dekeyser R 1988 *Phys. Rev.* B **38** 6941
[12] Kopinga K, Delica T and Leschke H 1989 *Phys. Rev.* B **40** 7239
Delica T and Leschke H 1990 *Physica* A **168** 736
[13] Blöte H W J 1975 *Physica* B **79** 427
[14] Kopinga K, Emmen J, De Vries G C, Lemmens L and Kamieniarz G 1988 *J. Physique* C **8** 1451
[15] Kamieniarz G 1988 *Phys. Rev.* B **38** 4873
[16] Campana L S, Caramico D'Auria A, Esposito U, Kamieniarz G and Dekeyser R 1990 *Phys. Rev.* B **42** 10765
[17] Pini M G and Rettori A 1984 *Phys. Rev.* B **29** 5246
[18] Gerling R W and Landau D P 1990 *Phys. Rev.* B **41** 7139
[19] Campana L S, Caramico D'Auria A, Esposito F, Esposito U and Kamieniarz G 1991 *Physica* B **168** 153
[20] Steiner M, Villain J and Windsor C G 1976 *Adv. Phys.* **25** 87
[21] Kamieniarz G and Vanderzande C 1987 *Phys. Rev.* B **35** 3341
[22] Riseborough P S 1983 *Solid State Commun.* **48** 901
[23] Kopinga K and de Jonge W J M *Magnetic Excitations and Fluctuations II* 1987 ed U Balucani, S W Lovesey, M G Rasetti and V Tognetti (Berlin: Springer) p 166
[24] Dupas C and Renard J P 1977 *J. Phys. C: Solid State Phys.* **10** 5057
[25] Kopinga K, de Neef T, de Jonge W J M and Gerstein B C 1976 *Phys. Rev.* B **13** 3953
[26] Steiner M and Dorner B 1990 *Europhys. Lett.* **12** 653
[27] Steiner M and Kjems J K 1977 *J. Phys. C: Solid State Phys.* **10** 2665
[28] Kopinga K private communication
[29] Steiner M and Dachs H 1974 *Solid State Commun.* **14** 841
[30] Villain J 1974 *J. Physique* **35** 27
[31] Lindgård P A and Kowalska A 1976 *J. Phys. C: Solid State Phys.* **9** 2081
[32] Grille H, Kamieniarz G and Gerling R W 1992 *J. Magn. Magn. Mater.* at press